AGU100 ADVANCING EARTH AND SPACE SCIENCE

Water Resources Research

RESEARCH ARTICLE
10.1029/2018WR022730

Key Points:
- Reactivity is enhanced by interface stretching and colalescence
- Taylor dispersion overestimates reactivity due to incomplete mixing at preasymptotic times
- Dispersive lamella approach captures the full mixing and reaction behavior

Correspondence to:
M. Dentz,
marco.dentz@csic.es

Citation:
Perez, L. J., Hidalgo, J. J., & Dentz, M. (2019). Upscaling of mixing-limited bimolecular chemical reactions in Poiseuille flow. *Water Resources Research*, *55*, 249–269. https://doi.org/10.1029/2018WR022730

Received 6 FEB 2018
Accepted 7 DEC 2018
Accepted article online 14 DEC 2018
Published online 8 JAN 2019

Upscaling of Mixing-Limited Bimolecular Chemical Reactions in Poiseuille Flow

Lazaro J. Perez[1,2,3], Juan J. Hidalgo[1,2], and Marco Dentz[1,2]

[1]Spanish National Research Council (IDAEA-CSIC), Barcelona, Spain, [2]Hydrogeology group (UPC-CSIC), Barcelona, Spain, [3]Department of Civil and Environmental Engineering, Technical University of Catalonia, Barcelona, Spain

Abstract We consider the fast irreversible bimolecular chemical reaction $A + B \rightarrow C$ in the Poiseuille flow through a channel, in which A displaces B. This system allows to systematically study the impact of the interaction of interface deformation and diffusion on mixing and reactive transport. At early times, the reaction is diffusion controlled. With increasing time, advection begins to dominate and we find enhanced reaction efficiency due to the deformation of the interface between the two reactants. For times larger than the characteristic diffusion time across the channel, mixing and reaction are quantified by the Taylor dispersion coefficient. Predictions based on Taylor dispersion may significantly overestimate the reaction efficiency at preasymptotic times, when the system is characterized by incomplete mixing. This type of behaviors of incomplete mixing and reaction have been observed in heterogeneous systems across different scales. Channel flow allows to study them in detail for a well-controlled system. We propose a dispersive lamella approach based on the concept of effective dispersion which accurately predicts the full evolution of the product mass. Specifically, this approach captures the impact of interface deformation and diffusive coalescence, which marks the transition to the Taylor regime. It gives insight into the mechanism of incomplete mixing and its consequences for reactive transport in more general porous media flows.

1. Introduction

The dynamics of reactive fronts and mixing interfaces is important for a wide range of natural processes from the biosphere to natural and anthropogenic contamination of aquifers. Natural aquifers exhibit heterogeneities that change the flow and transport dynamics. Heterogeneity modifies the topology of reactive fronts and mixing interfaces, which leads to chemical reaction dynamics that are very different from the ones observed in the laboratory under well-mixed equilibrium conditions (de Anna, Jimenez-Martinez, et al., 2014; Gramling et al., 2002; Raje & Kapoor, 2000) and the ones predicted by the transport laws for homogeneous media (Dentz et al., 2011; Li et al., 2006; Steefel et al., 2005).

Chemical species must physically come into contact one with another for chemical reactions to occur. Mixing, the process by which different substances originally segregated tend to occupy the same volume, is what makes this contact possible. Mixing controls biogeochemical transformations that are fast compared to mass transfer, such as dissolution, precipitation, or degradation (Li et al., 2006; Mariani et al., 2010; Simoni et al., 2007). Mass transfer limitations induced by medium heterogeneity causes reduced reaction and mixing efficiency compared to equivalent homogeneous medium descriptions based on hydrodynamic dispersion or macrodispersion (Gramling et al., 2002; Li et al., 2006; Luo et al., 2008; Tartakovsky et al., 2009). On the other hand, mixing due to medium heterogeneity increases reaction compared to mixing by diffusion only (de Anna, Dentz, et al., 2014; Jiménez-Martínez et al., 2015; Rolle et al., 2009).

Traditionally, Darcy-scale reactive transport has been described by the advection-dispersion-reaction equation (ADRE; Dentz et al., 2011; Steefel et al., 2005), which expresses species mass conservation due to advective-dispersive mass transfer and chemical reaction as

$$\phi \frac{\partial c_i(\mathbf{x},t)}{\partial t} = -\nabla \cdot \left[\mathbf{q} c_i(\mathbf{x},t) - \mathbf{D}\nabla c_i(\mathbf{x},t)\right] - r_i(\mathbf{x},t,\{c_j(\mathbf{x},t)\}), \quad (1)$$

where ϕ is porosity, c_i is the concentration of reactant i, $\mathbf{q}$ is Darcy velocity, $\mathbf{D}$ is the dispersion tensor, and r_i is the local reaction rate of species i, which in general may depend explicitly on position, time, and concentrations of all reacting species $\{c_j\}$. Reaction rates are typically estimated from laboratory experiments under well-mixed conditions in batch or flow-through reactors (Dentz et al., 2011; Luo et al., 2008; Steefel et al., 2005).

Their use in (1) is subject to the existence of a well-mixed support volume and to mass transfer on the support scale being much faster than the chemical reaction. The first condition implies that the microscopic Peclét number, which compares the diffusion and advection time scales on the support scale, needs to be smaller than 1. The second condition implies that the microscopic Damköhler number, which compares characteristic mass transfer to reaction times, needs to be smaller than 1 (Battiato & Tartakovsky, 2011). A variety of laboratory (de Anna, Jimenez-Martinez, et al., 2014; Gramling et al., 2002; Kapoor et al., 1998; Raje & Kapoor, 2000) and field studies (Davis et al., 2000; Hess et al., 2002) have shown that the ADRE overestimates the reaction efficiency. This may be traced back to the fact that the above conditions are often not fulfilled; this means locally the system is not well mixed and the mass transfer time scales are larger than the reaction time scales.

Laboratory and numerical experiments have shown that enhanced chemical reactivity can be linked to deformation of mixing interfaces (de Anna, Dentz, et al., 2014; de Anna, Jimenez-Martinez, et al., 2014; Le Borgne et al., 2014). Lamellar approaches have been long used for the quantification of mixing and reaction in spatially variable flow fields (Duplat et al., 2010; Duplat & Villermaux, 2008; Le Borgne et al., 2013, 2014, 2015; Ranz, 1979; Villermaux & Duplat, 2003). They are based on the concept that a heterogeneous concentration distribution can be represented by an ensemble of noninteracting lamellae, on which diffusion is enhanced through compression of the lamella due to flow deformation. Duplat and Villermaux (2008), Villermaux (2012), and Le Borgne et al. (2013) have extended this approach for random flows to account for interactions between lamellae based on random coalescence. These approaches provide models for the mixing and reaction behaviors in the deformation and coalescence regimes.

In this paper, we study the impact of flow variability on the reaction efficiency of an instantaneous irreversible bimolecular chemical reaction $A + B \rightarrow C$. This relatively simple reaction can be seen as the building stone of more complex chemical reactions such as metabolic activity of a biofilm (Steefel et al., 2005) or remediation of water contamination by anthropogenic elements such as sulfides (Batens & Van Keer, 2003) and ammonia (Garg et al., 2000). It is an elementary reaction that allows to study in detail the impact of the fundamental mechanisms of flow deformation and diffusion on mixing and chemical reaction. We consider the laminar flow through a channel, which is characterized by the parabolic Poiseuille profile. This flow scenario serves as a model system for flow through open fractures, laminar reactors, single pores, and capillaries. This system has been studied experimentally by Kapoor et al. (1998), who emphasized the impact of concentration fluctuations around the vertical mean on the prediction of the overall reactivity. These authors considered the breakthrough of product concentration in order to characterized the system reactivity. While the flow field here is deterministic, it exhibits transport and mixing features typical for heterogeneous flow fields, such as the evolution of effective and apparent dispersion coefficients toward a macrodispersion, the Taylor dispersion coefficient, and front spreading due to spatially variable advection. In fact, as we will see in the following, the reaction behavior shows features that are well-known consequences of incomplete mixing of the (macroscopic) support scale. Thus, even though the system is idealized, it allows studying the fundamental mechanisms of incomplete mixing and chemical reaction in heterogeneous systems. Thus, the developed approaches and conclusions also apply to more general, heterogeneous flow situations.

In order to study the detailed dispersion and reaction behavior, we use a numerical reactive random walk particle tracking (RWPT; Alhashmi et al., 2015; Benson & Meerschaert, 2008; Edery et al., 2009, 2010; Zhang et al., 2013) to determine the evolution of the species concentrations and the global reactivity in terms of the total product mass. The mixing behavior is characterized in terms of effective dispersion, which measures the average width of a point injection in the channel cross section, or in other words, the Green function of the transport problem (Dentz & Carrera, 2007). Based on this concept, we propose a dispersive lamella approach to quantify the impact of mixing on chemical reaction.

The paper is organized as follows. In section 2 we describe the reactive transport problems. Section 3 discusses the results of reactive RWPT simulations in the Poiseuille flow. Section 4 determines the product evolution based on stretched lamellae and proposes the dispersive lamella approach to capture the full evolution of reactivity including stretching-enhanced mixing and coalescence.

2. Methodology

We consider the irreversible bimolecular chemical reaction

$$A + B \xrightarrow{k} C, \tag{2}$$

where k denotes the reaction rate coefficient. This elementary reaction can be considered as a constituent of more complex reactions, which can be built as combinations of bimolecular and unimolecular reactions (Gillespie, 2000).

2.1. Reactive Transport

In this paper, we focus on the impact of mass transfer due to spatially variable advection and diffusion on chemical reaction, which is described by the following advection-diffusion reaction equation (ADRE):

$$\frac{\partial c_i(\mathbf{x},t)}{\partial t} + \nabla\cdot\mathbf{v}(\mathbf{x})c_i(\mathbf{x},t) - D\nabla^2 c_i(\mathbf{x},t) = -kc_A(\mathbf{x},t)c_B(\mathbf{x},t) \tag{3a}$$

$$\frac{\partial c_C(\mathbf{x},t)}{\partial t} + \nabla\cdot\mathbf{v}(\mathbf{x})c_C(\mathbf{x},t) - D\nabla^2 c_C(\mathbf{x},t) = kc_A(\mathbf{x},t)c_B(\mathbf{x},t) \tag{3b}$$

for $i = A, B$, where $\mathbf{v}(\mathbf{x})$ is the flow velocity. As outlined in section 1, this formulation requires that the support scale underlying this continuum description be well-mixed and that the microscopic Damköhler number be smaller than 1; this means that the support volume is considered a well-mixed reactor. The global reaction behavior is characterized by the evolution of the total mass of the reaction product

$$m_C(t) = \int \mathrm{d}\mathbf{x}\, c_C(\mathbf{x},t). \tag{4}$$

By integration of (3b) over the flow and transport domain, we obtain

$$\frac{\mathrm{d}m_C(t)}{\mathrm{d}t} = R(t), \qquad R(t) = \int \mathrm{d}\mathbf{x}\, kc_A(\mathbf{x},t)c_B(\mathbf{x},t), \tag{5}$$

where $R(t)$ is the reaction rate. We consider initially segregated A and B, which are distributed according to

$$c_A(\mathbf{x},t=0) = c_0\mathbb{I}(-L \le x < 0), \qquad c_B(\mathbf{x},t=0) = c_0\mathbb{I}(0 \le x < L), \tag{6}$$

where L is the initial extension of the domain occupied by A and B species, and $\mathbb{I}(\cdot)$ is an indicator function, which is equal to 1 if the argument is true and 0 else. The C species is initially nonexistent.

2.1.1. Constant Flow

As a reference case, we consider first the constant flow velocity $\mathbf{v}(\mathbf{x}) = v\mathbf{e}_x$, with $\mathbf{e}_x$ the unit vector in x direction. Furthermore, the chemical reaction is assumed to be fast; this means that c_0k, with c_0 a characteristic concentration, is larger than the characteristic transport rate $1/\tau_v$, where $\tau_v = 2D/v^2$ is the time after which advective displacements are larger than diffusive. This criterion can be expressed by the Damköhler number which compares the reaction to the transport rate, $Da = c_0k\tau_v$, and corresponds to $Da \gg 1$ in the following. In a domain infinitely extended in 1 direction, with the initial conditions (6) for $L \to \infty$, the product concentration is given by(Gramling et al., 2002)

$$c_C(x,t) = \frac{c_0}{2}\mathrm{erfc}\left(\frac{|x-vt|}{2\sqrt{Dt}}\right), \tag{7}$$

see also Appendix C1. Note that Gramling et al. (2002) considered an inflow boundary condition, for which this solution is only approximate, while for the initial value problem posed above it is exact. The product mass is given by

$$m_C(t) = 2c_0\sqrt{\frac{2}{\pi}}\sigma(t),\ \sigma(t) = \sqrt{2Dt}, \tag{8}$$

where $\sigma(t)$ is the interface width. The scaling of the product mass as $\sqrt{t}$ can be understood as follows. Since the reaction is instantaneous, the reaction rate $R(t)$ is equal to the diffusive mass flux at the interface between the two species, which is $j_D \approx Dc_0/\sqrt{2Dt}$, where c_0 is the concentration difference across the interface and $\sqrt{2Dt}$ its width. Thus, one obtains from (5), $m_c(t) \approx c_0\sqrt{2Dt}$. This solution serves as the reference for the behaviors observed for spatially variable flow. Appendix C1 develops analytical solutions for the initial conditions (6).

2.1.2. Poiseuille Flow

In this paper, we focus on mixing and reaction in the laminar flow through a two-dimensional channel, which is a model for mixing and reaction in flow through a single pore, open fractures, and laminar flow reactors, for example. The half width of the channel is denoted by a; the channel walls are impervious and represent no-slip boundaries for the flow. Thus, the flow velocity is aligned with the channel axis and depends only on the coordinate perpendicular to the channel orientation, $\mathbf{v}(\mathbf{x}) = u(y)\mathbf{e}_x$. The speed $u(y)$ is given by the parabolic Poiseuille profile

$$u(y) = v_0\left(1 - \frac{y^2}{a^2}\right), \tag{9}$$

where v_0 is the maximum flow velocity. The mean flow velocity across the channel is given by $v_m = 2v_0/3$. The A and B species are initially segregated according to (6), and the C species is nonexistent. At the horizontal domain boundaries at $y = \pm a$ the solute flux is 0. Under these conditions, there is no closed form analytical solution. Thus, the reactive transport problem (3) is solved numerically using a reactive RWPT method (Perez et al., 2018), whose analysis and implementation are presented in the next section. Kapoor et al. (1998) studied a similar system, namely, reactive transport in parabolic pipe flow, using laboratory experiments and numerical simulations, which gives qualitatively similar results to the ones reported in the following.

Transport can be characterized by the diffusion time across the channel diameter $\tau_D = (2a)^2/2D$ and the characteristic advection time $\tau_v = 2D/v_m^2$, which measures the time at which longitudinal advective and diffusive displacements are equal. For times $t < \tau_v$ diffusion is the dominant transport process; for $t > \tau_v$ advection starts dominating. These time scales define the Péclet number

$$Pe = \sqrt{\frac{\tau_D}{\tau_v}} = \frac{v_m a}{2D}. \tag{10}$$

If $Pe \ll 1$, diffusion is the dominant transport mechanism and the particles mix completely over the channel cross section before advection starts to impact on the longitudinal particle displacement. For $Pe \gg 1$, the solute mixes across the channel after an advective profile along the flow field (9) has been established. The Damköhler number here compares the characteristic advection time τ_v to the characteristic reaction time $1/c_0 k$,

$$Da = c_0 k \tau_v. \tag{11}$$

The *DaPe* number for this system is given by

$$DaPe = c_0 k \tau_D. \tag{12}$$

It compares the mixing time across the channel cross section to the characteristic reaction time. For $DaPe \gg 1$, the system is characterized by incomplete mixing.

2.2. Numerical Simulations

In the following, we briefly describe the numerical reactive RWPT method used to solve the reactive transport problem, and the numerical setup.

2.2.1. RWPT

The numerical simulations are based on RWPT combined with a probabilistic rule for the reaction. The equation that governs the advective-diffusive motion of particles belonging to the A, B, and C species is the Langevin equation (Risken, 1996)

$$\frac{\mathrm{d}\mathbf{x}(t)}{\mathrm{d}t} = \mathbf{v}[\mathbf{x}(t)] + \sqrt{2D}\boldsymbol{\xi}(t), \tag{13}$$

where $\mathbf{x}(t)$ is the trajectory of a particle and $\boldsymbol{\xi}(t)$ is a vectorial Gaussian white noise characterized by zero mean $\langle \boldsymbol{\xi}(t) \rangle = \mathbf{0}$ and covariance $\langle \xi_i(t)\xi_j(t') \rangle = \delta_{ij}\delta(t - t')$, where δ_{ij} is the Kronecker delta. The flow velocity is $\mathbf{v}(\mathbf{x}) = u(y)\mathbf{e}_x$ with $u(y)$ given by (9). No flux boundary conditions at the horizontal channel boundaries at $y = \pm a$ are implemented through reflection of particles.

The Langevin equation (13) is discretized using an Euler scheme as

$$\mathbf{x}(t + \Delta t) = \mathbf{x}(t) + \mathbf{v}[\mathbf{x}(t)]\Delta t + \sqrt{2D\Delta t}\boldsymbol{\eta}(t), \tag{14}$$

where the $\eta(t)$ are independent identically distributed Gaussian random variables characterized by 0 mean and unit variance. At each time step, the position of each particle is recorded and the distance between a given A and B particle is calculated. We describe the point of view of a B particle; the one of an A particle is analogous. The survival probability $P_s[\mathbf{x}(t)]$ of a B particle in the time interval $[t, t + \Delta t]$ depends on the number $N_A[\mathbf{x}(t)]$ of A particles within a well-mixed volume ΔV centered at the position $\mathbf{x}(t)$ of a B particle(Perez et al., 2018) as

$$P_s[\mathbf{x}(t)] = \exp\left[-p_r(\Delta t)N_A[\mathbf{x}(t)]\right], \tag{15}$$

where $p_r(\Delta t) = k\Delta t/(N_0\Delta V)$ is the probability for a single reaction event, and N_0 is the total number of particles. The local reaction volume $\Delta V = \pi r^2$, where the reaction radius is chosen as $r = \sqrt{24D\Delta t}$ (Benson & Meerschaert, 2008). The impact of the choice of the reaction radius on the overall reaction behavior is studied in Perez et al. (2018). The occurrence of a reaction event is determined through a Bernoulli trial based on

Table 1
Parameters Applied on the Reactive RWPT Model

	$Pe = 14$	$Pe = 48$	$Pe = 96$
D (m^2/s)	$2 \cdot 10^{-6}$	$4.5 \cdot 10^{-7}$	$2.25 \cdot 10^{-7}$
v_0 (m/s)	$8.5 \cdot 10^{-3}$	$6.5 \cdot 10^{-3}$	$6.5 \cdot 10^{-3}$
N_0	$6 \cdot 10^5$	10^6	$3 \cdot 10^6$

Note. RWPT = random walk particle tracking.

the survival probability (15). If the reaction occurs, the B particle and the closest A particle are removed and a particle C is placed at the middle point of the A and B particle locations. Note that these details on removal of A and B and placing the C particles have no impact on the simulated reaction behavior or the equivalence of the particle scheme with the ADRE derived in the previous section. The motion of the produced C particles follows (14). The total number of C particles, or total mass, is calculated as

$$m_C(t) = N_c(t), \tag{16}$$

where $N_c(t)$ is the number of C particles at time t. The equivalence between this reactive RWPT method and the Eulerian reactive transport formulation (3) and its validation can be found in Perez et al. (2018). Appendix A discusses the impact of finite particle numbers on the product mass. Based on this assessment, the simulations use a total number of $N_0 > 10^6$ particles.

In order to illustrate the concentration fields formed by the particles in the RWPT model, we use an adaptive Gaussian kernel density estimator (Botev et al., 2010),

$$c_i(\mathbf{x}, t) = \sum_{p=1}^{N_c(t)} K_h\left(\mathbf{x} - \mathbf{x}_{p,i}(t)\right), \tag{17}$$

where $i = A, B, C$, $\mathbf{x}_{p,i}(t)$ is the location of the pth particle of species i, and $K_h(\mathbf{x})$ is a Gaussian probability density function of mean $\mathbf{0}$ and variance h^2. The bandwidth h is determined according to the procedure detailed in Botev et al. (2010). Note that other authors have used kernel density estimators for accurate predictions on local solute mixing and reactive transport in case of limited particle numbers (Fernàndez-Garcia & Sanchez-Vila, 2011; Rahbaralam et al., 2015; Sole-Mari et al., 2017). The reactive random walk simulation according to the algorithm described above does not require kernel density estimators. In fact, we make sure that the particle number is sufficiently high to avoid finite size effects, as discussed in Appendix A. Here the reconstruction of the concentration fields with kernel density estimator is only used to illustrate the concentration distributions of the reacting species.

2.2.2. Numerical Setup

We consider here three advection-dominated transport scenarios with $Pe = 14$, 48, and 96 whose specific parameters are detailed in Table 1. The Damköhler number is for all scenarios $Da > 5$ such that reactions at times larger than τ_v can be considered instantaneous. The $DaPe$ number is $DaPe > 70$. Thus, reactive transport is strongly affected by incomplete mixing and the system cannot be considered well mixed for a wide range of times. The reactive transport problem is solved with the RWPT simulator described in the previous section. As initial condition, we consider uniform areal distributions of A and B particles from $x = -3 \cdot 10^{-1}$ to $x = 0$ m and $x = 0$ to $x = 3 \cdot 10^{-1}$ m, respectively. The characteristic reaction time is $1/c_0 k = 10^{-2}$ s; the time step is $\Delta t = 10^{-2}$ s. The reaction radius is equal to $r = \sqrt{24 D \Delta t}$. Note that the chosen diffusion coefficients are high with respect to the values of solutes in water but comparable to the ones reported for nonaqueous phase liquid contaminants (Lee & Chrysikopoulos, 1995). The number of particles required to suppress finite size effects (this means artificial incomplete mixing) depends on the Péclet number; see also Appendix A.

2.3. The Lamella Concept and Effective Dispersion

In this section, we briefly summarize the concept of the stretched lamella (Ranz, 1979) to quantify the concentration content of a solute under the action of advection and diffusion. Then we present an alternative approach, termed here the dispersive lamella based on the concept of effective dispersion (Dagan, 1990;

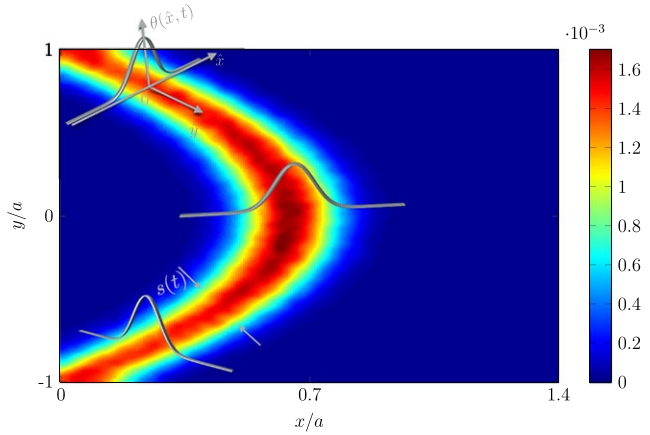

Figure 1. Illustration of the stretched lamella approach (after Villermaux, 2012). The lamella elongates due to flow deformation and mixes due to diffusion. The concentration profile across a lamella is Gaussian shaped. The concentration map is obtained by random walk particle tracking for a line injection, $Pe = 96$ at $t = 20\tau_v$.

Dentz & Carrera, 2007; Dentz et al., 2000; Kitanidis, 1988). To this end, we consider an instantaneous line injection perpendicular to the direction of flow in the channel; this means $c(\mathbf{x}, t = 0) = \delta(x)/2a$. The concentration $c(\mathbf{x}, t)$ can be represented in terms of the Green function $g(\mathbf{x}, t|y')$ as

$$c(\mathbf{x}, t) = \frac{1}{2a}\int_{-a}^{a} \mathrm{d}y' g(\mathbf{x}, t|y'), \tag{18}$$

where $g(\mathbf{x}, t|y')$ satisfies

$$\frac{\partial g(\mathbf{x}, t|y')}{\partial t} + u(y)\frac{\partial g(\mathbf{x}, t|y')}{\partial x} - D\nabla^2 g(\mathbf{x}, t|y') = 0 \tag{19}$$

for the initial condition $g(\mathbf{x}, t|y') = \delta(x)\delta(y-y')$ and no-flux boundary conditions at the horizontal boundaries. The lamellar approaches discussed in the following can be seen as approximations for the Green function $g(\mathbf{x}, t|y')$, for which in general no closed form analytical solution can be found.

2.3.1. The Stretched Lamella

In order to quantify the impact of fluid deformation and the associated mixing behavior on chemical reactions, Ranz (1979) developed the lamellae method. This method has been the basis for the quantification of mixing and reaction in heterogeneous flow fields (Bandopadhyay et al., 2017; de Anna, Jimenez-Martinez, et al., 2014; Duplat & Villermaux, 2008; Le Borgne et al., 2013, 2014; Meunier & Villermaux, 2010; Ranz, 1979; Villermaux, 2012). The lamella approach decomposes the material line into a set of noninteracting infinitesimal linear line segments (lamellae), which are transported purely advectively, are deformed by the action of the flow field, and mix with the ambient fluid due to diffusion as illustrated in Figure 1. The concentration content along the parabolic front is determined by diffusion and the local shear deformation. The concentration in the center, where the shear deformation is minimum, is much lower than at the sides where shear is increasing. The stretched lamella approach, described in the following, approximates the Green function $g(\mathbf{x}, t|y')$.

First, the advection-diffusion problem is transformed into the coordinate system of a purely advectively transported strip, which deforms and rotates according to the flow action; see Figure 1. A strip located at the vertical position y' moves with the constant velocity $u(y')$ and deforms and rotates due to shear action $\alpha(y') = \mathrm{d}u(y')/\mathrm{d}y'$. The coordinate transform is

$$\hat{\mathbf{x}} = \mathbf{A}^{\top}(t|y')\left[\mathbf{x} - \mathbf{x}_a(t|y')\right], \mathbf{x}_a(t|y') = \begin{bmatrix} u(y')t \\ y' \end{bmatrix}, \tag{20}$$

where $\mathbf{A}(t|y')$ is the orthogonal matrix

$$\mathbf{A}(t|y') = \frac{1}{\lambda(t)^2}\begin{bmatrix} \alpha(y')t & -1 \\ 1 & \alpha(y')t \end{bmatrix}, \tag{21}$$

which rotates into the coordinate system, whose $\hat{x}$ axis is perpendicular to the strip. Note that the strip orientation and length are given by

$$\delta\mathbf{z}(t|y') = \delta y \begin{pmatrix} \alpha(y')t \\ 1 \end{pmatrix}, \lambda(t|y') = \frac{|\delta\mathbf{z}(t|y')|}{\delta y'} = \sqrt{1+\alpha(y')^2t^2}, \tag{22}$$

where $\delta y'$ is the infinitesimal initial strip length. The Green function $g(\mathbf{x}, t|y')$ is expressed in terms of the Green function $\hat{g}(\hat{\mathbf{x}}, t|y')$ in the moving coordinate system as

$$g(\mathbf{x}, t|y') = \hat{g}\left(\mathbf{A}^{\top}(t|y')\left[\mathbf{x} - \mathbf{x}_a(t|y')\right], t|y'\right). \tag{23}$$

By inserting the latter into equation (19), we obtain after some algebra

$$\frac{\hat{g}(\hat{\mathbf{x}}, t|y')}{\partial t} + \epsilon(t|y')\hat{\mathbf{x}} \cdot \nabla\hat{g}(\hat{\mathbf{x}}, t|y') - D\nabla^2\hat{g}(\hat{\mathbf{x}}, t|y') = 0, \tag{24}$$

where $\epsilon(t|y')$ is the deformation rate tensor in the moving coordinate system,

$$\epsilon(t|y') = \frac{1}{\lambda(t)^2}\begin{bmatrix} \alpha(y')^2t & \alpha(y')^3t^2 - \alpha(y') \\ 0 & -\alpha(y')^2t \end{bmatrix}. \tag{25}$$

Typically mass transfer across the strip is disregarded and the Green function only depends on the coordinate $\hat{x}$ perpendicular to the strip,

$$\hat{g}(\hat{\mathbf{x}}, t|y') = \lambda(t|y')\theta(\hat{x}, t|y')\delta(y - y'), \tag{26}$$

where $\theta(\hat{x}, t|y')$ satisfies

$$\frac{\partial\theta(\hat{x}, t|y')}{\partial t} - \gamma(t|y')\hat{x}\frac{\partial\theta(\hat{x}, t|y')}{\partial\hat{x}} - D\frac{\partial^2\theta(\hat{x}, t|y')}{\partial\hat{x}^2} = 0. \tag{27}$$

The elongation rate $\gamma(t|y')$ is defined by

$$\gamma(t|y') = \frac{1}{\lambda(t|y')}\frac{\mathrm{d}\lambda(t|y')}{\mathrm{d}t} = \frac{\alpha(y')^2t}{1+\alpha(y')^2t^2}. \tag{28}$$

Note that in this approach, the lamellae do not sample the transverse velocity contrast and do not interact. They are independent. They displace due to advection only and mix due to stretching-enhanced diffusion. Dispersion of the interface in this approach is ballistic because each lamella moves at its own constant velocity $u(y')$.

Here we approximate the shear rate $\alpha(y)$ by its vertical average

$$\alpha(y) \approx \overline{\alpha} = \frac{1}{2a}\int_{-a}^{a}\mathrm{d}y\,\alpha(y) = \frac{v_0}{a}. \tag{29}$$

In this approximation, $\gamma(t|y') = \gamma(t)$, $\lambda(t|y') = \lambda(t)$, and $\theta(\hat{x}, t|y') = \theta(\hat{x}, t)$ are independent from y'. Equation (27) is the basis for the lamellar reaction model used in section 4. The chemical reaction is solved for a single lamella, and the overall reactivity is obtained by integration over all stretched lamellae.

We emphasize that the stretched lamella approach is based on noninteracting lamellae; this means that the merging of lamellae due to transverse diffusion and the sampling of the vertical flow contrast are not taken into account in this model. Each lamella remains on its initial streamline. Thus, when one considers the overall dispersion of the line, it increases ballistically because each line segment moves at its initial velocity $u(y')$. This approximation fails at times that are of the order of the diffusion time over the channel cross section, $\tau_D = (2a)^2/2D$.

2.3.2. The Dispersive Lamella

Here we present an alternative approach based on the concept of effective dispersion to account for the action of transverse diffusion. In the stretched lamella approach, the concept of the lamella describes a material element that deforms and diffuses in the flow field. In the dispersive lamella approach proposed here, the lamella describes a material element that disperses as a result of the diffusive sampling of the vertical velocity contrast. This concept is illustrated in Figure 2, which shows the evolution of the Green function $g(\mathbf{x}, t|y')$ from point sources at different positions in the channel cross section. As pointed out above, the plumes close to the channel boundaries are more deformed and thus disperse more than those located in the center. This deformation is accounted for in the stretched lamella approach. With increasing time, however, a lamella samples the velocity contrast across the channel cross section due to transverse diffusion and eventually covers

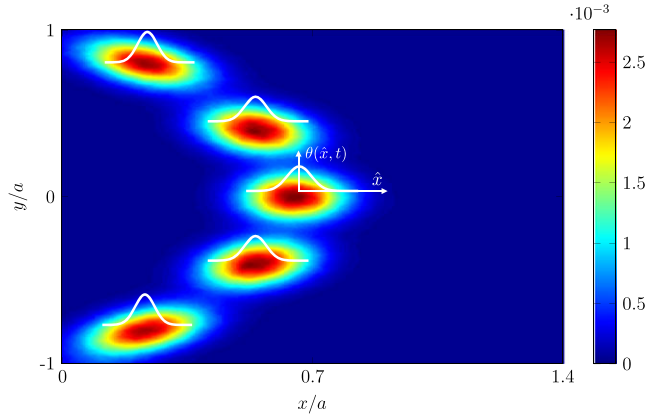

Figure 2. Illustration of the dispersive lamella approach. Concentration $g(\mathbf{x}, t|y')$ evolving from point injections at $y' = -0.8, -0.5, 0, 0.5$, and $0.8\,a$ at $t = 20\tau_v$ for $Pe = 96$. The concentration profile across a lamella is a Gaussian whose width is described by $\sigma_e(t)$.

the whole cross section as shown in Figure 3. This mechanism, which leads to the phenomenon of Taylor dispersion, is not accounted for in the stretched lamella approach.

Here instead of transformation into the coordinate system of a purely advectively transported strip, we transform into the coordinate system that moves with the center of mass $m(t|y')$ of the Green function $g(\mathbf{x}, t|y')$. The position vector in the transformed system is thus

$$\hat{\mathbf{x}} = \begin{bmatrix} x - m(t|y') \\ y \end{bmatrix}, \qquad m(t|y') = \int \mathrm{d}\mathbf{x}\, x g(\mathbf{x}, t|y'). \tag{30}$$

The Green function then reads in terms of the Green function $\hat{g}(\hat{\mathbf{x}}, t|y')$ as

$$g(\mathbf{x}, t|y') = \hat{g}[x - m(t|y'), y, t|y']. \tag{31}$$

Inserting the latter into equation (19), we obtain

$$\frac{\partial \hat{g}(\hat{\mathbf{x}}, t|y')}{\partial t} + v'(y, t|y')\frac{\partial^2 \hat{g}(\hat{\mathbf{x}}, t|y')}{\partial \hat{x}^2} - D\hat{\nabla}^2 \hat{g}(\hat{\mathbf{x}}, t|y') = 0, \tag{32}$$

where $v'(t|y')$ is the velocity fluctuation around the center of mass velocity,

$$v'(y, t|y') = u(y) - v(t|y'), \qquad v(t|y') = \frac{m(t|y')}{\mathrm{d}t}. \tag{33}$$

Transformation into the coordinate system that evolves with the center of mass velocity $v(t|y')$ guarantees that the effect of transverse diffusion on the interface shape is accounted for correctly. Recall that the stretched

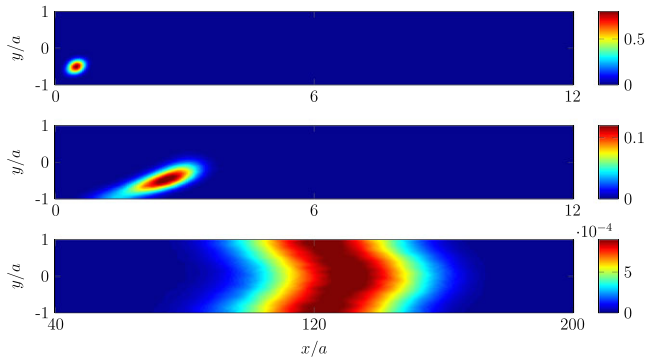

Figure 3. Evolution of the concentration distribution $g(\mathbf{x}, t|y')$ evolving from a point injection at $y' = -0.5\,a$ at (top to bottom) $t = 3.5, 70\ \tau_v$, and τ_D for $Pe = 62$.

lamella approach gives a ballistic interface evolution at all times. In order to account for the impact of diffusive sampling of the vertical velocity contrast on the interface evolution, we approximate $\hat{g}(\hat{\mathbf{x}}, t|y')$ by the following projection

$$\hat{g}(\hat{\mathbf{x}}, t|y') \approx G(y, t|y')\theta(\hat{x}, t|y'), \tag{34}$$

where $\theta(\hat{x}, t|y')$ is the vertically integrated concentration defined by

$$\theta(\hat{x}, t|y') = \int_{-a}^{a} \mathrm{d}y\, \hat{g}(\hat{\mathbf{x}}, t|y'), \tag{35}$$

and

$$G(y, t|y') = \int_{-\infty}^{\infty} \mathrm{d}\hat{x}\, \hat{g}(\hat{\mathbf{x}}, t|y') \tag{36}$$

is the Green function for transverse diffusion. The vertically integrated $\theta(\hat{x}, t|y')$ ratifies the transport equation

$$\frac{\partial\theta(\hat{x}, t|y')}{\partial t} - D^e(t|y')\frac{\partial^2\theta(\hat{x}, t|y')}{\partial\hat{x}^2} = 0; \tag{37}$$

see Appendix B. The effective dispersion coefficient $D^e(t|y')$ describes the rate of change of the variance of $g(\mathbf{x}, t|y')$ in flow direction,

$$D^e(t|y') = \frac{1}{2}\frac{\mathrm{d}\sigma^2(t|y')}{\mathrm{d}t}, \qquad \sigma^2(t|y') = \int \mathrm{d}\mathbf{x}\, \left[x - m(t|y')\right] g(\mathbf{x}, t|y'). \tag{38}$$

Equation (37) characterizes the concentration content of a dispersive lamella, which deforms due to the action of the flow field and disperses due to vertical sampling of the flow variability by transverse diffusion as illustrated in Figures 2 and 3. Thus, it accounts for the diffusive sampling across the cross section which is disregarded by the stretched lamella approach.

Exact analytical expressions for $m(t|y')$ and $\sigma^2(t|y')$ can be found in Dentz and Carrera (2007). Note that $m(t|y') = v(y')t$ at $t \ll \tau_D$ and $m(t|y') = v_m t$ at $t \gg \tau_D$. Similarly, $\sigma^2(t|y') = 2Dt$ for $t \ll \tau_D$ and $\sigma^2(t|y') = 2Dt + 2\mathcal{D}t$ for $t \gg \tau_D$, where $\mathcal{D} = 2v_m^2 a^2/105D$ is the Taylor dispersion coefficient (Taylor, 1953). The effective dispersion coefficient $D^e(t|y')$ has been studied in detail in Dentz and Carrera (2007). In the following, we approximate $D^e(t|y')$ by its average over the channel cross section,

$$D^e(t) = \frac{1}{2a}\int_{-a}^{a} \mathrm{d}y' D^e(t|y'). \tag{39}$$

Thus, $\theta(\hat{x}, t|y') = \theta(\hat{x}, t)$ is independent from y'. The effective dispersion coefficient represents the average dispersion of the initial line source. The corresponding effective variance is

$$\sigma_e^2(t) = \frac{1}{2a}\int_{-a}^{a} \mathrm{d}y' \sigma^2(t|y'). \tag{40}$$

The effective dispersion coefficient $D^e(t)$ can be written as (Dentz & Carrera, 2007)

$$D^e(t) = 2D^a(t) - D^a(2t), \tag{41}$$

where $D^a(t)$ is the apparent dispersion coefficient. It is obtain from the apparent variance $\sigma_a^2(t)$

$$\sigma_a^2(t) = \frac{1}{2a}\int_{-a}^{a} \mathrm{d}y' \int \mathrm{d}\mathbf{x}\, (x - v_m t)^2 g(\mathbf{x}, t|y'), \tag{42}$$

which measures the spread of the solute distribution $c(\mathbf{x}, t)$ about its center of mass position $v_m t$. The apparent dispersion coefficient $D^a(t)$ is defined in analogy to (38) as

$$D^a(t) = \frac{1}{2}\frac{\mathrm{d}\sigma_a^2(t)}{\mathrm{d}t}. \tag{43}$$

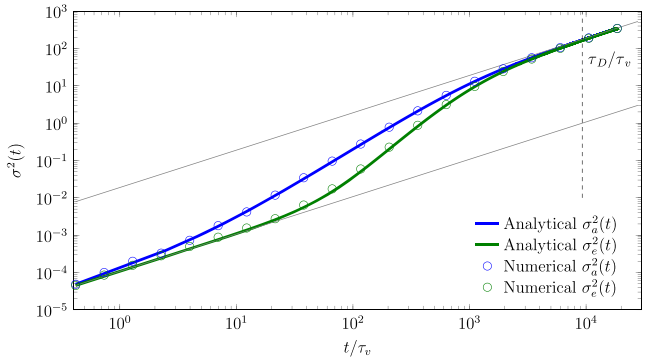

Figure 4. Evolutions of $\sigma_a^2(t)$ and $\sigma_e^2(t)$ from random walk particle tracking (symbols) and the analytical approximations (44) and (45) (solid lines) for the setup characterized by $Pe = 96$. The grey solid lines denote the limits behaviors $2Dt$ (lower) and $2(D + \mathcal{D})t$ (upper).

As a consequence of (41), the effective variance $\sigma_e^2(t)$ can be written as

$$\sigma_e^2(t) = 2\sigma_a^2(t) - \frac{\sigma_a^2(2t)}{2}. \tag{44}$$

We obtain an explicit analytical expression for $D^e(t)$ by noting that Haber and Mauri (1988) developed the following analytical expression for $\sigma_a^2(t)$ for two-dimensional laminar flow

$$\sigma_a^2(t) = 2Dt + 2\mathcal{D}t\left(1 - \frac{1 - e^{-\phi\frac{\pi^2 Dt}{4a^2}}}{\phi\frac{\pi^2 Dt}{4a^2}}\right), \tag{45}$$

where $\phi = (n + 1)^2$ with n the number of symmetry planes of the flow, and $\mathcal{D}$ is the Taylor dispersion coefficient.. For the channel flow under consideration here $\phi = 4$. Using the approximation (45) in (41) and (44) gives explicit expressions for the effective dispersion coefficient and variance.

Figure 4 shows the evolution of the effective and apparent variances $\sigma_e^2(t)$ and $\sigma_a^2(t)$ determined from numerical random walk simulations and the analytical expressions based on (45). At early times for $t < \tau_v$ both variances behave in the same way as $2Dt$. For increasing times, $\tau_v < t < \tau_D$, $\sigma_a^2(t)$ grows faster than $\sigma_e^2(t)$ due to advective deformation (spreading) of the solute front. When $t > \tau_D$ both variances converge toward the same behavior of $2(D + \mathcal{D})st$. The analytical solutions compare well with the numerical data.

Equation (37) with $D^e(t|y') = D^e(t)$ is the basis for the dispersive lamella approach employed in section 4 for the prediction of reactive transport. The reactive transport problem is solved for a single dispersive lamella. The overall reactivity is then obtained by integration over all dispersive lamellae that evolve from the initial solute distribution.

3. Mixing and Reaction in the Flow Through a Channel

In this section, we study mixing and reaction in channel flow for the scenarios described in section 2.2.2. Figure 5 shows the concentration maps of reactant *A* and product *C* for $Pe = 96$. The evolution of the product mass is shown in Figure 6 for the three *Pe* under consideration. The evolution of the reaction front is governed by the competition between diffusive expansion and the deformation caused by the velocity field. At early times, $t \leq \tau_v$, molecular diffusion controls the chemical reaction through mass transfer across the interface (de Anna, Dentz, et al., 2014; de Anna, Jimenez-Martinez, et al., 2014; Raje & Kapoor, 2000). The distribution of the product concentration is uniform in the vertical direction, and it behaves according to (7) along x. The product mass in this regime increases diffusively according to (8) as illustrated in Figure 6.

For increasing times $\tau_v \leq t \ll \tau_D$, the interface deforms following the parabolic velocity profiles, and its shape is described by $x_f(y, t) = u(y)t$. The interface length increases, and as a result the global reactivity increases. Flow variability enhances the reaction efficiency compared to uniform flow as pointed out by Kapoor et al. (1998). The impact of deformation of the mixing front is analogous to observations made at the Darcy scale in heterogeneous flows (de Barros et al., 2012; Le Borgne et al., 2014).

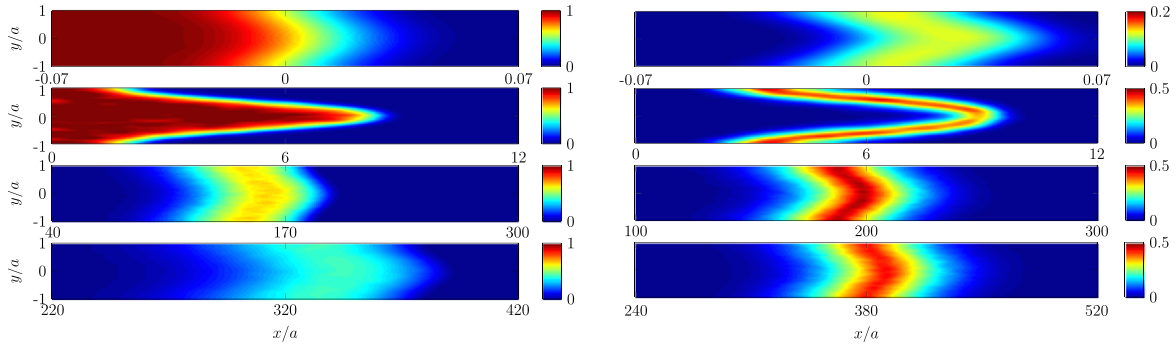

Figure 5. Concentration maps of (left column) A and (right column) C at times (top to bottom) $t = 0.4$, 290 τ_v, τ_D, and $2\tau_D$ for $Pe = 96$.

For times $\tau_v \ll t \leq \tau_D$, the interface length decreases due to diffusive mixing across the channel, which may be seen as the diffusive coalescence of the lamellar segments that make up the interface (see also the discussion in de Anna, Jimenez-Martinez, et al., 2014). The growth rate of the product mass decreases. For times $t \gg \tau_D$, the interface straightens and the system can be considered well mixed in the cross section of the channel. The interface width can be described by the Taylor dispersion coefficient (Taylor, 1953), which here is given by $\mathcal{D} = 2v_m^2 a^2/105D$. Taylor dispersion quantifies the impact of the interplay of interface deformation and diffusive coalescence on asymptotic mixing. Despite the finiteness of the initial distributions of A and B, mass production is well described by (8) for $D = \mathcal{D}$ as illustrated in Figure 6. This is further discussed in the next section. Note that extrapolation of the asymptotic behavior to preasymptotic times $t < \tau_D$ may significantly overestimate the reactivity. The reason is that at times $\tau_v < t < \tau_D$ the system is characterized by incomplete mixing. In the following, we investigate the quantification of the evolution of the reaction efficiency with emphasis on stretching and coalescence behavior during the intermediate time regime $\tau_v < t < \tau_D$ and the transition to the asymptotic Taylor regime.

4. Incomplete Mixing

As pointed out in the previous section, the asymptotic reactive transport description in terms of the Taylor dispersion coefficient does not quantify properly the chemical reaction at preasymptotic times, for which the species concentrations are not fully mixed transversely. In the following, we first apply the stretched lamella approach to account for the impact of the deformation of the interface between the A and B species on the overall reactivity. Then, we develop an approach, termed the dispersive lamella, to capture the full reaction behavior, which relies on the concept of effective dispersion (Dagan, 1990; Dentz et al., 2000; Kitanidis, 1988). This approach relies on the quantification of the effective interface width and its evolution and accounts for both stretching-enhanced mixing and diffusive coalescence.

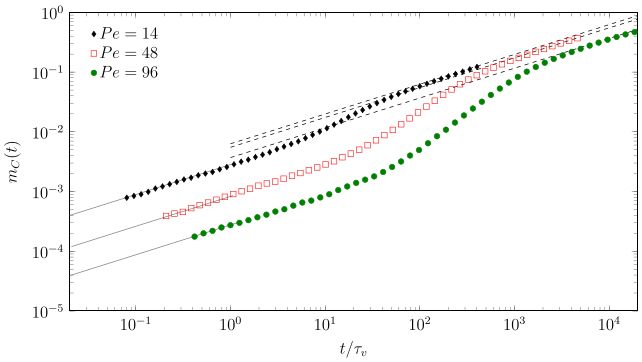

Figure 6. The evolution of $m_C(t)$ obtained from reactive random walk particle tracking for different Pe is shown by symbols. The early time estimation of the product mass evolution (8) is shown by solid lines; the late time evolution given by (8) parameterized by the Taylor dispersion coefficient $\mathcal{D}$ is denoted by dashed lines.

4.1. The Stretched Lamella

We first model the system reactivity using the stretched lamella approach, which describes the evolution of concentration by equation (27), where we set $\alpha = \overline{\alpha}$ such that $\gamma(t|y') = \gamma(t)$. Thus, reaction and diffusion across a single lamella are described by (see also Bandopadhyay et al., 2017)

$$\frac{\partial \theta_i(\hat{x},t)}{\partial t} - \gamma(t)\hat{x}\frac{\partial \theta_i}{\partial \hat{x}} + D\frac{\partial^2 \theta_i(\hat{x},t)}{\partial \hat{x}^2} = -k\theta_A(\hat{x},t)\theta_B(\hat{x},t) \tag{46a}$$

$$\frac{\partial \theta_C(\hat{x},t)}{\partial t} - \gamma(t)\hat{x}\frac{\partial \theta_i}{\partial \hat{x}} + D\frac{\partial^2 \theta_C(\hat{x},t)}{\partial \hat{x}^2} = k\theta_A(\hat{x},t)\theta_B(\hat{x},t), \tag{46b}$$

where $\hat{x}$ is the direction perpendicular to the direction of stretching, D stands for the diffusion coefficient, and $i = A, B$. This problem can be solved for fast reactions, which gives for the concentration of C

$$\theta_C(\hat{x},t) = \frac{2ac_0}{2}\mathrm{erfc}\left[\frac{|\hat{x}|}{\sqrt{2s(t)}}\right]; \tag{47}$$

for $L \to \infty$ in the initial conditions (6), see Appendix C2. The concentration of C in the strip coordinate system is obtained by using (26) as

$$c_C(\hat{x},t) = \frac{1}{2a}\int_{-a}^{a} \mathrm{d}y'\,\lambda(t|y')\theta_C(\hat{x},t)\delta(y-y') = \lambda(t)\frac{c_0}{2}\mathrm{erfc}\left[\frac{|\hat{x}|}{\sqrt{2s(t)}}\right]. \tag{48}$$

The total product mass is then given by integration over space according to (4), which gives for the total mass

$$m_C(t) = c_0\sqrt{\frac{2}{\pi}}\ell(t)s(t), \tag{49}$$

where $\ell(t) = 2a\lambda(t)$ is the interface length and $s(t)$ its width. Corrections to the species concentration and product mass due to the fact that L is finite here are discussed in Appendix C2. The interface length and width are approximately given by

$$\ell(t) = 2a\sqrt{1+\overline{\alpha}^2t^2}, \qquad s(t) = \sqrt{\frac{2D(t+\overline{\alpha}^2t^3/3)}{1+\overline{\alpha}^2t^2}}. \tag{50}$$

Note that $\ell(t)s(t)$ measures the area of the mixing zone. At times $t \ll \overline{\alpha}^{-1}$ expression (49) reduces to (8) for reaction-diffusion in uniform flow. For $t \gg \overline{\alpha}^{-1}$, expression (49) predicts that

$$m_C(t) = 2c_0a\overline{\alpha}\sqrt{\frac{4D}{3\pi}}t^{3/2}. \tag{51}$$

The prediction (49) of the product mass is illustrated in Figure 7 for $Pe = 48$ and 96. We omit the data for $Pe = 14$ because it behaves qualitatively in the same way while the time scales τ_D and τ_v are less separated. The stretched lamella model predicts the early time behavior and the behavior in the intermediate regime for $t \ll \tau_D$. Note that the lamellar reaction model is based on independent lamella. As soon as the individual strips start interacting due to diffusion across the channel, the prediction (49) breaks down. In the following, we will present an approach that accounts for the full evolution of the product mass.

4.2. The Dispersive Lamella

The approach outlined in the previous section considers elementary units, lamellae, which make up the initial interface. These lamellae are independent, and mass transfer across these noninteracting elementary units is due to diffusion and the local deformation action of the flow field. As discussed in section 4, the dispersive lamella considers point elements that make up the initial interface and follow their advective-diffusive motion in the flow field. In this approach, the evolution of the solute concentration is described by (37). Thus, the evolution of the species concentrations due to reactions at the interface is given by

$$\frac{\partial \theta_i(\hat{x},t)}{\partial t} - D^e(t)\frac{\partial^2 \theta_i(\hat{x},t)}{\partial \hat{x}^2} = -k\theta_A(\hat{x},t)\theta_B(\hat{x},t), \tag{52a}$$

$$\frac{\partial \theta_C(\hat{x},t)}{\partial t} - D^e(t)\frac{\partial^2 \theta_C(\hat{x},t)}{\partial \hat{x}^2} = k\theta_A(\hat{x},t)\theta_B(\hat{x},t) \tag{52b}$$

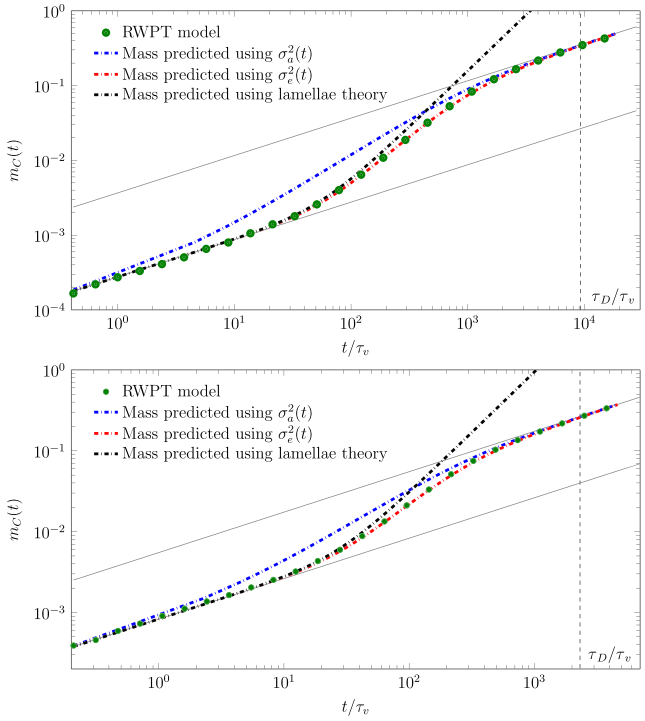

Figure 7. Evolution of $m_C(t)$ for (top) $Pe = 96$ and (bottom) $Pe = 48$ from reactive RWPT (symbols), from the dispersive lamella (55) parameterized by (blue dash-dotted line) the apparent variance $\sigma_a^2(t)$ and (red dash-dotted lines) the effective variance $\sigma_e^2(t)$. The black dash-dotted line denotes the evolution of $m_C(t)$ obtained from the stretched lamella (49). RWPT = random walk particle tracking.

for $i = A, B$, where we set the effective dispersion coefficient $D^e(t|y') = D^e(t)$ as discussed in section 4. For the initial conditions (6) with $L \to \infty$, the concentration of C across the lamella is given by

$$\theta_C(\hat{x}, t) = \frac{2ac_0}{2}\,\mathrm{erfc}\left[\frac{|\hat{x}|}{\sqrt{2\sigma_e(t)}}\right]; \tag{53}$$

see Appendix C3. Using expression (34), we obtain for the concentration of C at the interface

$$c_C(\hat{x}, t) = \frac{1}{2a}\int_{-a}^{a} \mathrm{d}y' G(y, t|y')\theta(\hat{x}, t) = \frac{c_0}{2}\,\mathrm{erfc}\left[\frac{|\hat{x}|}{\sqrt{2\sigma_e(t)}}\right]. \tag{54}$$

The total mass of C produced is obtained by integration of (53) according to (4) as

$$m_C(t) = 2c_0\sqrt{\frac{2}{\pi}}a\sigma_e(t); \tag{55}$$

see also (8). The area of the mixing zone here is given by $2a\sigma_e(t)$. Recall that $\sigma_e(t)$ is a measure for the effective interface width. Corrections due to the finiteness of L are discussed in Appendix C3.

Figure 7 shows the evolution of the product mass obtained from the numerical random walk simulations and the analytical estimate (55) from the dispersive lamella approach for $Pe = 48$ and 96. As shown in Figure 6 the behavior for $Pe = 14$ is qualitatively similar, but the transition regime of incomplete mixing is short. Thus, we omit these data here. The dispersive lamella approach gives equally good results for this case.

We have also plotted the evolution of product mass for an interface that evolves with the apparent width $\sigma_a(t)$, For $t < \tau_v$ diffusion dominates and all three approaches agree with the simulations results. For times $\tau_v < t \ll \tau_D$, the stretched and dispersive lamellae provide a good description of the product mass evolution. The interface model based on $\sigma_a(t)$ overestimates the product mass because it overestimates the interface width as discussed above. For times $\tau_v \ll t < \tau_D$, the stretched lamella model fails to predict the simulation data because it does not account for the diffusive interaction of individual strips. The dispersive lamella on

the other hand describes the reaction behavior well also in this interaction regime. In the late time regime $t \gg \tau_D$, both the dispersive lamella model and the interface model based on $\sigma_a(t)$ describe the data very well, while the stretched lamella model fails to match the data. Note that, despite the finite extensions of the initial species concentrations, the solution (55) provides a very good estimate even though the distribution of the A species is notably disperse as shown in Figure 5. As shown in Appendix C3, expression (55) provides a good solution for finite initial extension L of the species concentration as long as $\sigma_e(t) \ll \sqrt{2}L$, which is the case for the times under consideration here. For larger times, the product mass eventually goes toward the constant $m_C(t) = 2aLc_0$, which means all the product species have been consumed. The dispersive lamella approach agrees with the simulation data at all times. In particular, it captures both stretching-enhanced mixing and the diffusive coalescence in the intermediate and late time regimes.

5. Conclusions

We quantify the impact of flow variability on a fast irreversible bimolecular reactions in Poiseuille flow through a channel. This system shows features of incomplete mixing known for more complex porous media flows, namely, the overestimation of the reaction efficiency by the use of macroscale dispersion coefficient, here the Taylor dispersion coefficient $\mathcal{D} = 2v_m^2 a^2/105D$ quantifies the macroscopic mixing effect that accounts for the interaction of flow variability and diffusion only when the channel cross section is completely mixed by transverse diffusion this means for times greater than the diffusive time scale over the channel cross section $2a$, $\tau_D = (2a)^2/2D$.

We distinguish three different preasymptotic behaviors, which are separated by the characteristics advection scale $\tau_v = 2D/v_m$ and the diffusion scale τ_D. The time scale τ_v measures the time at which longitudinal advective and diffusive displacements are equal. At times smaller $t < \tau_v$, the product mass increases $\sim \sqrt{Dt}$ as in a constant plug flow reactor. Mixing and reaction are due to diffusion only. For increasing times $\tau_v < t \ll \tau_D$ the reaction behavior is dominated by the deformation of the diffuse interface, or equivalently the stretching of the independent lamellae that constitute the interface. The linear growth of the interface length together with the diffusive increase of its width leads to $m_C(t) \sim t^{3/2}$. Then at later times for $\tau_v \ll t < \tau_D$, the lamellae that form the interface start interacting, or coalescing, which marks the crossover to the Taylor regime for which $m_C(t) \sim \sqrt{(D + \mathcal{D})t}$. Note that on the one hand, we observe an increase of reactivity due to the variability of velocity compared to uniform flow and diffusion only. On the other hand, we observe the consequences of incomplete mixing because the asymptotic Taylor dispersion coefficient overestimates the reactivity. Similar phenomena have been observed for reactive transport on the Darcy scale, where the hydrodynamic dispersion coefficient turns out to overestimate the system reactivity (Gramling et al., 2002; Li et al., 2006; Luo et al., 2008; Tartakovsky et al., 2009). This emphasizes the importance of incomplete mixing and the correct quantification of it for the sound modeling of macroscale reactive transport in heterogeneous flows in general.

The stretched lamella approach (Duplat et al., 2010; Duplat & Villermaux, 2008; Le Borgne et al., 2013, 2014, 2015; Ranz, 1979; Villermaux & Duplat, 2003) is able to quantify the impact of interface deformation and accounts for the impact of preasymptotic incomplete mixing on the system reactivity. The stretched lamella approach can be see as an approximation to the Green function of the advection-diffusion problem in the channel. It considers diffusion and advection in the coordinate system attached to an advectively transported material element, which, upon linearization of the advection term, renders an exactly solvable model, which depends on the local deformation properties of the flow field and diffusion. As this model is based on independent lamellae, it does not account for the impact of transverse diffusion on the interface evolution and thus cannot account for the full evolution of reactivity.

We develop a dispersive lamella approach, which describes the full temporal evolution of the reaction product accurately. Like the stretched lamella approach, the developed model is based on an approximation of the Green function for the advection-diffusion problem. Here, however, we transform into the coordinate system moving with the center of mass velocity of a partial plume representing the Green function. The impact of transverse diffusion on the interface evolution is quantified through a projection operation, which includes vertical averaging across the channel cross section. From this projection emerges an effective equation for the evolution of the Green function which is characterized by the effective dispersion coefficient, which describes the average growth rate of the width of the Green function. In fact, in the moving coordinate system, the evolution of the Green function is governed by a dispersion equation characterized by the time-dependent effective dispersion coefficient $D^e(t)$, which accounts for both stretching-enhanced diffusion at early times

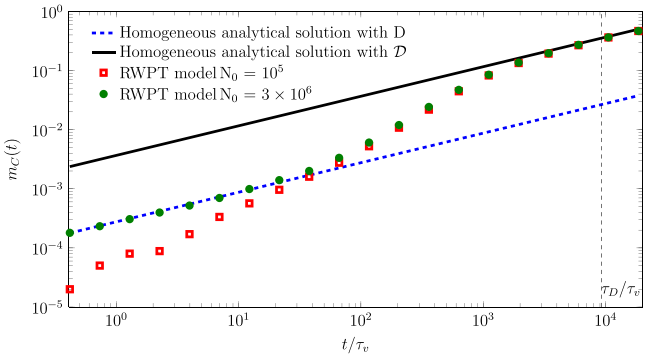

Figure A1. Evolution of $m_C(t)$ for different particle numbers. Expression (8) with (dashed line) D and (solid line) $\mathcal{D}$ predict the early and later time behavior of $m_C(t)$, respectively. RWPT = random walk particle tracking.

and front coalescence at late times. Based on an analytical expression for $D^e(t)$, the dispersive lamella quantifies the full evolution of the product mass and particularly the stretching and coalescence processes in a single modeling framework.

The proposed approach can be generalized straightforwardly to three dimensions and randomly stratified porous media, for which expressions for the effective and apparent dispersion coefficients exist both for infinite and confined media (Bolster et al., 2011; Güven et al., 1984; Fiori & Dagan, 2002; Matheron & de Marsily, 1980; Zavala-Sanchez et al., 2009). Furthermore, the fact that asymptotic (macro) dispersion, here Taylor dispersion, overestimates mixing and reaction (incomplete mixing) has been observed in porous media on the pore and Darcy scales (e.g., Dentz et al., 2011; Gramling et al., 2002). Due to this analogy, the findings and modeling approaches in terms of effective dispersion may have an impact for effective reactive transport modeling in heterogeneous flows in a range of applications.

Appendix A: Finite Size Effects in Modeling the Reaction

We illustrate the impact of the total particle number in the chemical reaction comparing the simulations for $Pe = 96$ for $3 \cdot 10^6$ particles and 10^5 particles. Figure A1 compares numerical data to the exact analytical solution (8) parameterized by D and $\mathcal{D}$, which is valid at early times $t \ll \tau_v$ and late times $t \gg \tau_D$. We find that at times $t \leq \tau_v$, when D controls the reaction, lower N_0 creates artificial concentration fluctuations due to fluctuations of particle numbers between subvolumes, which simulates an artificial incomplete mixing. Thus, reactivity may be underestimated as a result of this effect. Clearly, the insufficient number of particles to model the reaction produces a loss in accuracy. This artificial effect must not be confused with the occurrence of true incomplete mixing. The data from the simulation with $N_0 = 3 \cdot 10^6$ particles accurately matches the analytical solution at early times. At intermediate times, $\tau_v \leq t \ll \tau_D$, where true, physical incomplete mixing dominates, the simulations at both N_0 behave similarly because the artificial incomplete mixing is overshadowed by the true physical effect. Similarly, at asymptotic times, both particle numbers give good estimates because Taylor dispersion is the result of the diffusive sampling of the cross-sectional velocity over time, which is less affected by a low particle number. In order to exclude artificial incomplete mixing and finite size effects, the reactive RWPT results are performed with $N_0 > 10^6$ particles. Note that the particle number necessary to avoid the effect of artificial incomplete mixing at early times depends on the Péclet number. For low Péclet numbers, particles explore a larger radius per random walk step $\propto \sqrt{2D\Delta t}$ and therefore mix faster locally than at high Péclet numbers. The physically well-mixed support volume is larger than for high Pe. Thus, for a lower total particle number, one has at low Pe the same number of particles inside a well-mixed support volume as for a higher particle number at high Pe for which the well-mixed support volume is much smaller.

Appendix B: The Dispersive Lamella

Here we briefly derive equation (37), which forms the basis for the dispersive lamella approach. We separate $\hat{g}(\hat{\mathbf{x}}, t|y')$ into the projection $G(y, t|y')\theta(\hat{x}, t|y')$ and fluctuations $\theta'(\mathbf{x}, t|y')$ about it such that

$$\hat{g}(\hat{\mathbf{x}}, t|y') = G(y, t|y')\theta(\hat{x}, t|y') + \theta'(\hat{\mathbf{x}}, t|y'). \tag{B1}$$

Inserting this decomposition into (32) gives

$$\frac{\partial G(y,t|y')\theta(\hat{x},t|y')}{\partial t}+\frac{\partial\theta'(\hat{\mathbf{x}},t|y')}{\partial t}+\left[u'(y)-v'(t|y')\right]G(y,t|y')\frac{\partial\theta(\hat{x},t|y')}{\partial\hat{x}}$$
$$=-\left[u'(y)-v'(t|y')\right]\frac{\partial\theta'(\hat{\mathbf{x}},t|y')}{\partial\hat{x}}+D\left(\frac{\partial^2}{\partial\hat{x}^2}+\frac{\partial^2}{\partial y^2}\right)\left[G(y,t|y')\theta(\hat{x},t|y')+\theta'(\hat{\mathbf{x}},t|y')\right], \tag{B2}$$

where we used that $v'(\hat{y},t|y')=u(y)-v(t|y')$, which can be written as $v'(\hat{y},t|y')=u(y)-v_m-[v(t|y')-v_m]\equiv u'(y)-v'(t|y')$. The fluctuation of the center of mass velocity $v'(t|y')$ is given by(Dentz & Carrera, 2007)

$$v'(t|y')=\int_{-a}^{a}\mathrm{d}y u'(y)G(y,t|y'). \tag{B3}$$

Furthermore, we note that the Green function $G(y,t|y')$ satisfies

$$\frac{\partial G(y,t|y')}{\partial t}-D\frac{\partial^2 G(y,t|y')}{\partial y^2}=0 \tag{B4}$$

for the initial condition $G(y,t=0|y')=\delta(y-y')$. This implies that

$$\frac{\partial G(y,t|y')\theta(\hat{x},t|y')}{\partial t}-D\frac{\partial^2}{\partial y^2}G(y,t|y')\theta(\hat{x},t|y')= \tag{B5}$$

$$G(y,t|y')\frac{\partial\theta(\hat{x},t|y')}{\partial t}+\theta(\hat{x},t|y')\left[\frac{\partial G(y,t|y')}{\partial t}-D\frac{\partial^2}{\partial y^2}G(y,t|y')\right] \tag{B6}$$

$$=G(y,t|y')\frac{\partial\theta(\hat{x},t|y')}{\partial t}. \tag{B7}$$

Thus, we can write equation (B2) as

$$G(y,t|y')\frac{\partial\theta(\hat{x},t|y')}{\partial t}+\frac{\partial\theta'(\hat{\mathbf{x}},t|y')}{\partial t}+\left[u'(y)-v'(t|y')\right]G(y,t|y')\frac{\partial\theta(\hat{x},t|y')}{\partial\hat{x}}$$
$$=-\left[u'(y)-v'(t|y')\right]\frac{\partial\theta'(\hat{\mathbf{x}},t|y')}{\partial\hat{x}}+D\frac{\partial^2}{\partial y^2}\theta'(\hat{\mathbf{x}},t|y')+D\frac{\partial^2}{\partial\hat{x}^2}\left[G(y,t|y')\theta(\hat{x},t|y')+\theta'(\hat{\mathbf{x}},t|y')\right]. \tag{B8}$$

Vertical integration gives

$$\frac{\partial\theta(\hat{x},t|y')}{\partial t}=-\int_{-a}^{a}\mathrm{d}y\left[u'(y)-v'(t|y')\right]\frac{\partial\theta'(\hat{\mathbf{x}},t|y')}{\partial\hat{x}}+D\frac{\partial^2}{\partial\hat{x}^2}\theta(\hat{x},t|y'). \tag{B9}$$

By subtracting the latter from equation (B9), we obtain for the fluctuation $\theta'(\hat{\mathbf{x}},t|y')$

$$\frac{\partial\theta'(\hat{\mathbf{x}},t|y')}{\partial t}-D\frac{\partial^2\theta'(\hat{\mathbf{x}},t|y')}{\partial y^2}=-\left[u'(y)-v'(t|y')\right]G(y,t|y')\frac{\partial\theta(\hat{x},t|y')}{\partial\hat{x}}, \tag{B10}$$

where we disregard terms of second order in the fluctuating quantities and diffusion in flow direction because transverse diffusion is the key sampling mechanism. By using the Green function $G(y,t|y')$ of vertical diffusion we can write $\theta'(\hat{\mathbf{x}},t|y')$ as

$$\theta'(\hat{\mathbf{x}},t|y')=-\int_{0}^{t}\mathrm{d}t'\int_{-a}^{a}\mathrm{d}y''\left[u'(y'')-v'(t'|y')\right]G(y,t-t'|y'')G(y'',t'|y')\frac{\partial\theta(\hat{x},t'|y')}{\partial\hat{x}}. \tag{B11}$$

Inserting this expression into the right side of (B2) gives

$$\frac{\partial\theta(\hat{x},t|y')}{\partial t}=\int_0^t \mathrm{d}t'\,\mathcal{K}(t,t'|y')\frac{\partial^2\theta(\hat{x},t'|y')}{\partial\hat{x}^2}+D\frac{\partial^2}{\partial\hat{x}^2}\theta(\hat{x},t|y'), \tag{B12}$$

where we defined the dispersion kernel by

$$\mathcal{K}(t,t'|y')=\int_{-a}^{a}\mathrm{d}y\int_{-a}^{a}\mathrm{d}y''\left[u'(y)-v'(t|y')\right]\left[u'(y'')-v'(t'|y')\right]G(y,t-t'|y'')G(y'',t'|y'). \tag{B13}$$

The latter can be written as

$$\mathcal{K}(t,t'|y')=\int_{-a}^{a}\mathrm{d}y''u'(y'')G(y'',t'|y')v'(t-t'|y'')-v'(t|y')v'(t'|y'), \tag{B14}$$

where we used (B3) and the Markov property of the Green function, which means that

$$\int_{-a}^{a}\mathrm{d}y''G(y,t-t'|y'')G(y'',t'|y')=G(y,t|y'). \tag{B15}$$

The time integral of $\mathcal{K}(t,t'|y')$ is equal to the effective dispersion coefficient $D^e(t|y')$ defined in Dentz and Carrera (2007)

$$\begin{aligned}D^e(t|y')&=\int_0^t\mathrm{d}t'\,\mathcal{K}(t,t'|y')\\&=\int_0^t\mathrm{d}t'\int_{-a}^{a}\mathrm{d}y''u'(y'')G(y'',t'|y')v'(t-t'|y'')-v'(t|y')\int_0^t\mathrm{d}t'v'(t'|y').\end{aligned} \tag{B16}$$

The memory term on the right side of (B12) can be localized in time for $t-t'\ll t$,

$$\frac{\partial\theta(\hat{x},t|y')}{\partial t}=\left[\int_0^t\mathrm{d}t'\,\mathcal{K}(t,t'|y')\right]\frac{\partial^2\theta(\hat{x},t|y')}{\partial\hat{x}^2}+D\frac{\partial^2}{\partial\hat{x}^2}\theta(\hat{x},t|y'), \tag{B17}$$

which gives equation (37) for the dispersive lamella.

Appendix C: Analytical Solution for a Finite initial Condition

We derive here analytical solutions for the initial conditions (6). In the following, we give analytical solutions for the species concentrations and the product mass for a homogeneous medium, the stretched lamella, and the dispersive lamella approaches. First we note that the concentrations $c_{AC}=c_A+c_B$ and $c_{BC}=c_B+c_C$ satisfy conservative advection-diffusion equations for the same initial conditions as c_A and c_B because c_C is initially 0. As we consider an instantaneous reaction, the A and B species cannot coexist, and thus, the product concentration is given by

$$c_C(x,t)=\min\left[c_{AC}(x,t),c_{BC}(x,t)\right], \tag{C1}$$

because $c_{AC}=c_C$ if $c_A<c_B$ and vice versa.

C1. Homogeneous Medium

Thus, for a homogeneous medium with $v(x)=v=$ constant, the solutions for c_{AC} and c_{BC} are

$$c_{AC}(x,t)=\frac{c_0}{2}\left[\mathrm{erfc}\left(\frac{x-vt}{\sqrt{4Dt}}\right)-\mathrm{erfc}\left(\frac{x+L-vt}{\sqrt{4Dt}}\right)\right] \tag{C2}$$

$$c_{BC}(x,t)=\frac{c_0}{2}\left[\mathrm{erfc}\left(\frac{x-L-vt}{\sqrt{4Dt}}\right)-\mathrm{erfc}\left(\frac{x-vt}{\sqrt{4Dt}}\right)\right]. \tag{C3}$$

The product concentration is given by c_{AC} for $x \geq vt$ and by c_{BC} for $x < vt$. In the limit $L \to \infty$, the concentration of C is given by (7). Thus, we obtain for the product mass $m_C(t)$

$$m_C(t) = \int_{-\infty}^{vt} \mathrm{d}x\, c_{BC}(x,t) + \int_{vt}^{\infty} \mathrm{d}x c_{AC}(x,t), \tag{C4}$$

which we can write because of symmetry as

$$m_c(t) = 2\int_{vt}^{\infty} \mathrm{d}x\, c_{AC}(x,t). \tag{C5}$$

Inserting (C3) gives

$$m_c(t) = c_0 \int_0^L \mathrm{d}x\, \mathrm{erfc}\left(\frac{x}{\sqrt{4Dt}}\right) = c_0\sqrt{4Dt}\int_0^{L/\sqrt{4Dt}} \mathrm{d}x\, \mathrm{erfc}(x). \tag{C6}$$

Performing the remaining integral, we obtain

$$m_C(t) = c_0\sqrt{\frac{4Dt}{\pi}}\left[1 - \exp(-4\tau_L/t) + \sqrt{4\pi\tau_L/t}\,\mathrm{erfc}(\sqrt{4\tau_L/t}\right], \tag{C7}$$

where we defined the diffusion time $\tau_L = L^2/D$ over the initial extension of the species. For $t \ll \tau_L$, the evolution of the product mass is essentially equal to the one for $L \to \infty$ and given by $m_C(t) = 2c_0\sqrt{Dt/\pi}$. For $t \gg \tau_L$ it behaves as

$$m_C(t) = c_0 L\left(1 - \frac{1}{\sqrt{4\pi t/\tau_L}}\right) + \ldots. \tag{C8}$$

C2. Stretched Lamella

The stretched lamella approach requires solution of the equation

$$\frac{\partial\theta(\hat{x},t)}{\partial t} - \gamma(t)\hat{x}\frac{\partial\theta(\hat{x})}{\partial\hat{x}} - D\frac{\partial\theta(\hat{x},t)}{\partial\hat{x}^2} = 0, \tag{C9}$$

where θ stands for the concentrations $\theta_{AC} = \theta_A + \theta_C$ and $\theta_{BC} = \theta_B + \theta_C$, respectively. In order to solve (C9), we consider the variable transform according to Ranz (1979),

$$z = \hat{x}\exp\left[\Gamma(t)\right], \qquad \Gamma(t) = \int_0^t \mathrm{d}t\,\gamma(t'), \tag{C10}$$

and

$$\eta(t) = \int_0^t \mathrm{d}t' \exp[2\Gamma(t)]. \tag{C11}$$

Note that

$$\exp[\Gamma(t)] = \lambda(t), \tag{C12}$$

where $\lambda(t)$ is given by (22). We set $\theta(\hat{x},t) = \theta_0[\hat{x}\lambda(t),\eta(t)]$, where $\theta_0(z,\eta)$ satisfies

$$\frac{\partial\theta_0(z,\eta)}{\partial\eta} - D\frac{\partial^2\theta_0(z,\eta)}{\partial z^2} = 0. \tag{C13}$$

The latter is a diffusion equation whose solution for the initial condition $\theta(z,\eta=0) = \mathbb{I}(-L_1 \leq z < L_2)$ is

$$\theta_0(z,\eta) = \frac{1}{2}\left[\mathrm{erfc}\left(\frac{z+L_1}{\sqrt{4D\eta}}\right) - \mathrm{erfc}\left(\frac{z-L_2}{\sqrt{4D\eta}}\right)\right]. \tag{C14}$$

Thus, we obtain for $\theta(\hat{x},t)$

$$\theta(\hat{x},t) = \frac{1}{2}\left[\mathrm{erfc}\left(\frac{\hat{x}_1 + L_1\lambda(t)^{-1}}{\sqrt{2s(t)^2}}\right) - \mathrm{erfc}\left(\frac{z - L_2\lambda(t)^{-1}}{\sqrt{2s(t)^2}}\right)\right], \tag{C15}$$

where we defined

$$s(t)^2 = 2D\lambda(t)^{-2}\int_0^t \mathrm{d}t'\,\lambda(t')^2. \tag{C16}$$

Using expression (28) with $\alpha(y') = \overline{\alpha}$ gives expression (50) for $s(t)$. We obtain $\theta_{AC}(\hat{z},t)$ and $\theta_{BC}(\hat{z},t)$ by setting in (C22) $L_1 = -L$ and $L_2 = 0$, and $L_1 = 0$ and $L_2 = L$, respectively. The solution (47) is obtained in the limit $L \to \infty$.

Along the same lines as in the previous section, we obtain for the product mass across a single stretched lamella

$$\delta m_C(t) = c_0\sqrt{\frac{2}{\pi}}\lambda(t)s(t)\left(1-\exp[-A(t)^2]+\sqrt{\pi}A(t)\mathrm{erfc}\,[A(t)]\right), \tag{C17}$$

where we defined $A(t) = L\exp[-\Gamma(t)]/\sqrt{2s(t)^2}$.

C3. Dispersive Lamella

The solution method is fully analogous to the previous section. The dispersive lamella approach requires solution of the equation

$$\frac{\partial\theta(\hat{x},t)}{\partial t} - D^e(t)\frac{\partial\theta(\hat{x},t)}{\partial\hat{x}^2} = 0, \tag{C18}$$

where θ stands for the concentrations $\theta_{AC} = \theta_A + \theta_C$ and $\theta_{BC} = \theta_B + \theta_C$, respectively. In order to solve (C9), we consider the variable transform

$$\eta(t) = \int_0^t \mathrm{d}t' D^e(t') \tag{C19}$$

and set $\theta(\hat{x},t) = \theta_0[\hat{x},\eta(t)]$, where $\theta_0(z,\eta)$ satisfies

$$\frac{\partial\theta_0(z,\eta)}{\partial\eta} - \frac{\partial^2\theta_0(\hat{x},\eta)}{\partial\hat{x}^2} = 0. \tag{C20}$$

The latter is a diffusion equation whose solution for the initial condition $\theta(\hat{x},\eta=0) = \mathbb{I}(-L_1 \le \hat{x} < L_2)$ is

$$\theta_0(\hat{x},\eta) = \frac{1}{2}\left[\mathrm{erfc}\left(\frac{\hat{x}+L_1}{\sqrt{4\eta}}\right) - \mathrm{erfc}\left(\frac{z-L_2}{\sqrt{4\eta}}\right)\right]. \tag{C21}$$

Thus, we obtain for $\theta(\hat{x},t)$

$$\theta(\hat{x},t) = \frac{1}{2}\left[\mathrm{erfc}\left(\frac{\hat{x}_1+L_1}{\sqrt{2\sigma_e^2(t)}}\right) - \mathrm{erfc}\left(\frac{\hat{x}_1-L_2}{\sqrt{2\sigma_e^2(t)}}\right)\right], \tag{C22}$$

where $\sigma_e^2(t)$ is given by (40). Along the same lines as above, we obtain for the product mass of a single dispersive lamella

$$\delta m_C(t) = c_0\sqrt{\frac{2}{\pi}}\sigma_e(t)\left(1-\exp[-A_e(t)^2]+\sqrt{\pi}A_e(t)\mathrm{erfc}\left[A_e(t)\right]\right), \tag{C23}$$

where we defined $A_e(t) = L/\sqrt{2\sigma_e(t)^2}$. The solutions (53) and (55) are obtained in the limit $L \to \infty$. Note the the product mass $m_C(t)$ can be approximated by the product mass for $L \to \infty$ as long as $A_e(t) \ll 1$; this means $\sigma_e(t) \ll \sqrt{2}L$.

Acknowledgments
We acknowledge the support of the European Research Council (ERC) through the project MHetScale (617511) and the Spanish Ministry of Economy, Industry and Competitiveness and the Eurpoean Regional Developement Fund (ERDF) (CGL2016-80022-R). The numerical data used in the article can be obtained by following the steps and using the parameter values detailed in the paper. We thank Alberto Bellin, Diogo Bolster, Editor Xavier Sanchez-Vila, Associate Editor Daniel Fernandez-Garcia, and two anonymous reviewers for their valuable comments and recommendations.

References

Alhashmi, Z., Blunt, M., & Bijeljic, B. (2015). Predictions of dynamic changes in reaction rates as a consequence of incomplete mixing using pore scale reactive transport modeling on images of porous media. *Journal of Contaminant Hydrology*, *179*, 171–181.

Bandopadhyay, A., Le Borgne, T., Méheust, Y., & Dentz, M. (2017). Enhanced reaction kinetics and reactive mixing scale dynamics in mixing fronts under shear flow for arbitrary damköhler numbers. *Advances in Water Resources*, *100*, 78–95.

Batens, N., & Van Keer, R. (2003). On a numerical relaxation method for a chemical reaction-diffusion problem with an instantaneous and irreversible reaction. *Chemical Engineering Science*, *58*(21), 4815–4822.

Battiato, I., & Tartakovsky, D. (2011). Applicability regimes for macroscopic models of reactive transport in porous media. *Journal of Contaminant Hydrology*, *120*, 18–26.

Benson, D. A., & Meerschaert, M. M. (2008). Simulation of chemical reaction via particle tracking: Diffusion-limited versus thermodynamic rate-limited regimes. *Water Resources Research*, *44*, w12201. https://doi.org/10.1029/2008WR007111

Bolster, D., Valdés-Parada, F. J., LeBorgne, T., Dentz, M., & Carrera, J. (2011). Mixing in confined stratified aquifers. *Journal of Contaminant Hydrology*, *120-121*, 198–212. https://doi.org/10.1016/j.jconhyd.2010.02.003

Botev, Z. I., Grotowski, J. F., & Kroese, D. P. (2010). Kernel density estimation via diffusion. *The Annals of Statistics*, *38*(5), 2916–2957.

Dagan, G. (1990). Transport in heterogenous porous formations: Spatial moments, ergodicity, and effective dispersion. *Water Resources Research*, *26*, 1287–1290.

Davis, J., Kent, D., Coston, J., Hess, K., & Joye, J. (2000). Multispecies reactive tracer test in an aquifer with spatially variable chemical conditions. *Water Resources Research*, *36*(1), 119–134. https://doi.org/10.1029/1999WR900282

de Anna, P., Dentz, M., Tartakovsky, A., & Le Borgne, T. (2014). The filamentary structure of mixing fronts and its control on reaction kinetics in porous media flows. *Geophysical Research Letters*, *41*, 4586–4593. https://doi.org/10.1002/2014GL060068

de Anna, P., Jimenez-Martinez, J., Tabuteau, H., Turuban, R., Le Borgne, T., Derrien, M., & Méheust, Y. (2014). Mixing and reaction kinetics in porous media: An experimental pore scale quantification. *Environmental Science & Technology*, *48*(1), 508–516. https://doi.org/10.1021/es403105b

de Barros, F. P., Dentz, M., Koch, J., & Nowak, W. (2012). Flow topology and scalar mixing in spatially heterogeneous flow fields. *Geophysical Research Letters*, *39*, L08404. https://doi.org/10.1029/2012GL051302

Dentz, M., Borgne, T. L., Englert, A., & Bijeljic, B. (2011). Mixing, spreading and reaction in heterogeneous media: A brief review. *Journal of Contaminant Hydrology*, *120-121*, 1–17. https://doi.org/10.1016/j.jconhyd.2010.05.002

Dentz, M., & Carrera, J. (2007). Mixing and spreading in stratified flow. *Physics of Fluids*, *19*(1), 017–107. https://doi.org/10.1063/1.2427089

Dentz, M., Kinzelbach, H., Attinger, S., & Kinzelbach, W. (2000). Temporal behavior of a solute cloud in a heterogeneous porous medium, 1, point-like injection. *Water Resources Research*, *36*(12), 3591–3604.

Duplat, J., Innocenti, C., & Villermaux, E. (2010). A nonsequential turbulent mixing process. *Physical Fluids*, *22*(3), 035–104. https://doi.org/10.1063/1.3319821

Duplat, J., & Villermaux, E. (2008). Mixing by random stirring in confined mixtures. *Journal of Fluid Mechanics*, *617*, 51. https://doi.org/10.1017/s0022112008003789

Edery, Y., Scher, H., & Berkowitz, B. (2009). Modeling bimolecular reactions and transport in porous media. *Geophysical Research Letters*, *36*, L02407. https://doi.org/10.1029/2008GL036381

Edery, Y., Scher, H., & Berkowitz, B. (2010). Particle tracking model of bimolecular reactive transport in porous media. *Water Resources Research*, *46*, W07524. https://doi.org/10.1029/2009WR009017

Fernàndez-Garcia, D., & Sanchez-Vila, X. (2011). Optimal reconstruction of concentrations, gradients and reaction rates from particle distributions. *Journal of Contaminant Hydrology*, *120-121*, 99–114. https://doi.org/10.1016/j.jconhyd.2010.05.001

Fiori, A., & Dagan, G. (2002). Transport of a passive scalar in a stratified porous medium. *Transport in porous media*, *47*(1), 81–98.

Garg, R., Nair, S., & Bhaskarwar, A. N. (2000). Mass transfer with instantaneous chemical reaction in finite gas–liquid systems. *Chemical Engineering Journal*, *76*(2), 89–98.

Gillespie, D. T. (2000). The chemical Langevin equation. *The Journal of Chemical Physics*, *113*(1), 297–306.

Gramling, C. M., Harvey, C. F., & Meigs, L. C. (2002). Reactive transport in porous media: A comparison of model prediction with laboratory visualization. *Environmental Science &, Technology*, *36*(11), 2508–2514. https://doi.org/10.1021/es0157144

Güven, O., Molz, F. J., & Melville, J. G. (1984). An analysis of macrodispersion in a stratified aquifer. *Water Resources Research*, *20*(10), 1337–1353.

Haber, S., & Mauri, R. (1988). Lagrangian approach to time-dependent laminar dispersion in rectangular conduits. Part 1. Two-dimensional flows. *Journal of Fluid Mechanics*, *190*, 201–215.

Hess, K. M., Davis, J. A., Kent, D. B., & Coston, J. A. (2002). Multispecies reactive tracer test in an aquifer with spatially variable chemical conditions, Cape Cod, Massachusetts: Dispersive transport of bromide and nickel. *Water Resources Research*, *38*(8), 1161. https://doi.org/10.1029/2001WR000945

Jiménez-Martínez, J., de Anna, P., Tabuteau, H., Turuban, R., Le Borgne, T., & Méheust, Y. (2015). Pore-scale mechanisms for the enhancement of mixing in unsaturated porous media and implications for chemical reactions. *Geophysical Research Letters*, *42*, 5316–5324. https://doi.org/10.1002/2015GL064513

Kapoor, V., Jafvert, C. T., & Lyn, D. A. (1998). Experimental study of a bimolecular reaction in Poiseuille flow. *Water Resources Research*, *34*(8), 1997–2004.

Kitanidis, P. K. (1988). Prediction by the method of moments of transport in heterogeneous formations. *Journal of Hydrology*, *102*, 453–473.

Le Borgne, T., Dentz, M., & Villermaux, E. (2013). Stretching, coalescence, and mixing in porous media. *Physical Review Letters*, *110*(20), 204–501.

Le Borgne, T., Dentz, M., & Villermaux, E. (2015). The lamellar description of mixing in porous media. *Journal of Fluid Mechanics*, *770*, 458–498.

Le Borgne, T., Ginn, T. R., & Dentz, M. (2014). Impact of fluid deformation on mixing-induced chemical reactions in heterogeneous flows. *Geophysical Research Letters*, *41*, 7898–7906. https://doi.org/10.1002/2014GL062038

Lee, K., & Chrysikopoulos, C. (1995). Numerical modeling of three-dimensional contaminant migration from dissolution of multicomponent NAPL pools in saturated porous media. *Environmental Geology*, *26*(3), 157–165.

Li, L., Peters, C. A., & Celia, M. A. (2006). Upscaling geochemical reaction rates using pore-scale network modeling. *Advances in Water Resources*, *29*(9), 1351–1370. https://doi.org/10.1016/j.advwatres.2005.10.011

Luo, J., Dentz, M., Carrera, J., & Kitanidis, P. (2008). Effective reaction parameters for mixing controlled reactions in heterogeneous media. *Water Resources Research*, *44*, W02416. https://doi.org/10.1029/2006WR005658

Mariani, M., Labas, M., Brandi, R., Cassano, A., & Zalazar, C. (2010). Degradation of a mixture of pollutants in water using the UV/H_2O_2 process. *Water Science and Technology*, *61*(12), 3026–3032.

Matheron, M., & de Marsily, G. (1980). Is transport in porous media always diffusive? *Water Resources Research*, *16*, 901–917.

Meunier, P., & Villermaux, E. (2010). The diffusive strip method for scalar mixing in two dimensions. *Journal of Fluid Mechanics*, *662*, 134–172.

Perez, L., Hidalgo, J., & Dentz, M. (2018). Reactive random walk particle tracking method to model bimolecular chemical reactions, manuscript submitted for publication.

Rahbaralam, M., Fernàndez-Garcia, D., & Sanchez-Vila, X. (2015). Do we really need a large number of particles to simulate bimolecular reactive transport with random walk methods? A kernel density estimation approach. *Journal of Computational Physics*, *303*, 95–104. https://doi.org/10.1016/j.jcp.2015.09.030

Raje, D. S., & Kapoor, V. (2000). Experimental study of bimolecular reaction kinetics in porous media. *Environmental science & technology*, *34*(7), 1234–1239.

Ranz, W. E. (1979). Applications of a stretch model to mixing, diffusion, and reaction in laminar and turbulent flows. *AIChE Journal*, *25*(1), 41–47.

Risken, H. (1996). *The Fokker-Planck equation*. New York: Springer Heidelberg.

Rolle, M., Eberhardt, C., Chiogna, G., Cirpka, O. A., & Grathwohl, P. (2009). Enhancement of dilution and transverse reactive mixing in porous media: Experiments and model-based interpretation. *Journal of Contaminant Hydrology*, *110*(3), 130–142.

Simoni, M. D., Sanchez-Vila, X., Carrera, J., & Saaltink, M. W. (2007). A mixing ratios-based formulation for multicomponent reactive transport. *Water Resources Research*, *43*, W07419. https://doi.org/10.1029/2006WR005256

Sole-Mari, G., Fernandez-Garcia, D., Rodriguez-Escales, P., & Sanchez-Vila, X. (2017). A KDE based random walk method for modeling reactive transport with complex kinetics in porous media. *Water Resources Research*, *53*, 9019–9039. https://doi.org/10.1002/2017WR021064

Steefel, C., Depaolo, D., & Lichtner, P. (2005). Reactive transport modeling: An essential tool and a new research approach for the Earth sciences. *Earth and Planetary Science Letters*, *240*(3-4), 539–558. https://doi.org/10.1016/j.epsl.2005.09.017

Tartakovsky, A., Tartakovsky, G., & Scheibe, T. (2009). Effects of incomplete mixing on multicomponent reactive transport. *Advances in Water Resources*, *32*(11), 1674–1679. https://doi.org/10.1016/j.advwatres.2009.08.012

Taylor, G. (1953). Dispersion of soluble matter in solvent flowing slowly through a tube. *Proceedings of the Royal Society of London A: Mathematical, Physical and Engineering Sciences*, 219, 186–203. https://doi.org/10.1098/rspa.1953.0139

Villermaux, E. (2012). Mixing by porous media. *Comptes Rendus Mécanique*, *340*(11-12), 933–943. https://doi.org/10.1016/j.crme.2012.10.042

Villermaux, E., & Duplat, J. (2003). Mixing as an aggregation process. *Physical Review Letters*, *91*(18), 184–501.

Zavala-Sanchez, V., Dentz, M., & Sanchez-Vila, X. (2009). Characterization of mixing and spreading in a bounded stratified medium. *Advance Water Resources*, *32*, 635–648.

Zhang, Y., Papelis, C., Sun, P., & Yu, Z. (2013). Evaluation and linking of effective parameters in particle-based models and continuum models for mixing-limited bimolecular reactions. *Water Resources Research*, *49*, 4845–4865. https://doi.org/10.1002/wrcr.20368